https://doi.org/10.5194/essd-2025-821
Preprint. Discussion started: 14 January 2026

Open Access Earth System Science Data Discussions

Improved global daily nitrogen dioxide concentrations from 2005 to 2023 derived using a deep learning approach

Jiangshan Mu[1,2#], Chenliang Tao[3,1#], Yuqiang Zhang[1*], Zhou Liu[1], Yingnan Zhang[4], Na Zhao[1], Bin Luo[1], Qionghui Zhou[1], Qingzhu Zhang[1], Hongliang Zhang[3], Likun Xue[1*]

[1]Environment Research Institute, Shandong University, 266237, Qingdao, China
[2]Nicholas School of the Environment, Duke University, 27708, Durham, USA
[3]Department of Environmental Science and Engineering, Fudan University, 200233, Shanghai, China
[4]Department of Earth System Science, University of California, Irvine, 92697, California, USA
[#]These authors contributed equally to this work

Correspondence to: Yuqiang Zhang (yuqiang.zhang@sdu.edu.cn), Likun Xue (xuelikun@sdu.edu.cn)

Abstract. Nitrogen dioxide (NO_2) is a critical air pollutant with significant environmental and human health impacts, yet global and long-term NO_2 datasets with daily continuity and fine spatial resolution remain limited. In this study, we construct a continuous global daily NO_2 concentration spanning from 2005 to 2023 at a 0.1-degree resolution using the advanced Air Transformer deep learning framework that integrates satellite observations, ground-based measurements, meteorological reanalysis, land-use information, and auxiliary geophysical variables. The resulting dataset shows robust performance across diverse regions and pollution regimes, with improved spatial consistency and reduced biases relative to existing global products. Based on this dataset, we characterize the spatiotemporal evolution of global NO_2 concentrations over the past two decades. Global annual mean NO_2 increased from 2005 to 2015, followed by a moderate decline during 2016–2019, a pronounced decrease in 2020 associated with COVID-19–related reductions in economic activity and transportation, and a partial rebound thereafter, reaching 3.38 ppbv in 2023. The Northern Hemisphere and tropical regions largely followed the global trend, whereas the Southern Hemisphere exhibited distinct behaviour, with relatively stable or declining NO_2 levels prior to 2015, a sharp decrease in 2020, and a stronger post-pandemic rebound during 2021–2023. As one of the global, multi-decadal NO_2 datasets with daily resolution, this dataset provides a valuable resource for air quality assessment, exposure analysis, and atmospheric model evaluation.

1 Introduction

Nitrogen dioxide (NO_2) is a key atmospheric pollutant that plays a central role in tropospheric chemistry and air quality, and has significant implications for public health and environmental sustainability (Health Effects Institute, 2024). As an important precursor of ground-level ozone (O_3) and secondary fine particulate matter ($PM_{2.5}$), NO_2 strongly influences atmospheric oxidation processes and regional pollution levels (Li et al., 2019; Xue et al., 2014). Anthropogenic combustion sources, including vehicle traffic, power generation, and industrial activities, dominate global NO_2 emissions and are highly concentrated in urban and industrialized regions, resulting in pronounced spatial and temporal variability in surface concentrations.

https://doi.org/10.5194/essd-2025-821
Preprint. Discussion started: 14 January 2026

At the global scale, NO_2 concentrations exhibit substantial regional differences driven by variations in emission intensity, energy structure, and economic activity. Rapid urbanization and industrial development have led to increasing NO_2 levels in many regions, while emission control policies and technological improvements have contributed to declines elsewhere. Understanding these contrasting regional trends requires long-term, spatially consistent observations that can capture both gradual changes and abrupt perturbations associated with large-scale events, such as sudden emission reductions.

Current efforts to characterize global NO_2 distributions remain constrained by limitations in data availability and modeling approaches. Ground-based monitoring networks, while essential, are unevenly distributed, with most stations concentrated in high-income urban areas (Huang et al., 2023; Cooper et al., 2022; Di et al., 2019; Huang et al., 2018). Chemical transport models and traditional statistical approaches, including land-use regression models, often face challenges in reproducing fine-scale spatial heterogeneity and long-term temporal variability at the global scale, particularly when observational constraints are limited.

Recent advancements in remote sensing and data-driven methodologies provide promising opportunities to overcome these challenges (Huang et al., 2023; Cooper et al., 2022; Di et al., 2019; Huang et al., 2018). Satellite observations, such as the Ozone Monitoring Instrument (OMI) and the TROPOspheric Monitoring Instrument (TROPOMI), offer near-global coverage of NO_2 concentrations (Sekiya et al., 2022; Levelt et al., 2006; Veefkind et al., 2012), while machine learning techniques facilitate the integration of diverse geophysical, atmospheric, and socio-economic datasets (Huang et al., 2023; Chan et al., 2021; Wong et al., 2021; Chi et al., 2022; Long et al., 2022). These innovations enable the development of high-resolution datasets that capture spatial and temporal variations in NO_2 exposure, providing critical insights into the extent and drivers of environmental inequality. However, existing approaches often suffer from several limitations, such as lacking the spatial and temporal resolution needed to accurately reflect local variations, or failing to incorporate essential geophysical and atmospheric parameters (Di et al., 2019).

To address these challenges, we have developed a comprehensive global daily NO_2 dataset spanning from 2005 to 2023 at a 0.1° resolution using the Air Transformer (AiT) deep learning method. By taking advantage of the unique strengths of AiT in predicting atmospheric pollutant concentrations which will be discussed later, and incorporating important geophysical, atmospheric, and socio-economic parameters, the model overcomes retrieval uncertainties and better captures local variations in NO_2 concentrations, resulting in a more accurate and comprehensive understanding of NO_2 dynamics on a global scale. This high-resolution dataset aims to provide more precise and reliable insights into NO_2 trends and their driving factors, thereby overcoming the shortcomings of previous studies. Using this dataset, we further analyze the spatial and temporal evolution of NO_2 concentrations at global and regional scales, offering a robust data foundation for studies of atmospheric composition and air quality dynamics.

https://doi.org/10.5194/essd-2025-821
Preprint. Discussion started: 14 January 2026

2 Materials and methods

2.1 Data Collection and Processing

Surface NO_2 measurements with hourly resolution from 2005 to 2023 were collected from approximately 7,021 ground-based monitoring stations worldwide, including China National Environmental Monitoring Centre (CNEMC), Environmental Protection Agency (EPA), European Environment Agency (EEA), Tropospheric Ozone Assessment Report database (TOAR), and Open Air Quality (OpenAQ). To create model labels, duplicate data were removed by retaining the highest priority measurements according to the specified order (CNEMC/EPA/EEA > TOAR > OpenAQ). The raw data underwent additional quality control measures, including removal of outliers such as negative values, duplicate values (occurring for more than three consecutive hours), and extreme values (exceeding the 99.9th percentile). Days with at least 18 valid hourly NO_2 measurements were identified to calculate the daily average for each monitoring site. To ensure consistency with auxiliary variables, all daily NO_2 measurements were adjusted to the Universal Time Coordinated (UTC) zone and then used for independent training and validation of the machine learning model.

To accurately predict NO_2 concentrations, we incorporated a total of 17 independent features derived from multiple data sources. Meteorological reanalysis data were obtained from the ECMWF Reanalysis v5 (ERA5) dataset, including boundary layer height (BLH), temperature (TEMP), wind speed (WS), dewpoint temperature (DEW), pressure (PRE), precipitation (PRECIP), evaporation (EVA), and long-wave solar radiation (LWSR), all at a spatial resolution of 0.25° × 0.25° for the period 2005-2023. These meteorological variables are known to play key roles in controlling pollutant dispersion, vertical mixing, chemical reaction rates, and surface–atmosphere exchanges, and therefore provide essential physical constraints for NO_2 prediction. Satellite data of tropospheric column NO_2, formaldehyde (HCHO), and O_3 were retrieved from the L3 level products in OMI instrument at a resolution of 0.25° × 0.25° for 2005-2018, and from the L2 level products in TROPOMI instrument at a finer resolution of 5.5 km × 3.5 km for 2019-2023, providing complementary chemical information related to NO_x emissions, photochemical activity, and oxidant levels.

To enable consistent long-term analysis and minimize discrepancies arising from differences in sensor characteristics, retrieval algorithms, horizontal resolution, and overpass time between OMI and TROPOMI, we applied a seasonal, grid-specific adjustment to OMI products using TROPOMI as a reference during their overlap period (2019–2022). This harmonization step is particularly important for long-term trend analyses, as uncorrected inter-sensor differences could introduce artificial discontinuities into the time series. Specifically, OMI observations for years without TROPOMI coverage were corrected according to

$$\Omega_{OMI_{adj}}(i, yr, m) = \Omega_{OMI}(i, yr, m) + \Delta\Omega_{weights}(i, m)\,, \quad (1)$$

where

$$\Delta\Omega_{weights}(i, m) = \frac{1}{n}\sum_{yr=2019}^{yr=2022}(\Omega_{TROPOMI}(i, yr, m) - \Omega_{OMI}(i, yr, m)\,, \quad (2)$$

https://doi.org/10.5194/essd-2025-821
Preprint. Discussion started: 14 January 2026

where $\Omega_{OMI_{adj}}(i, yr, m)$, $\Omega_{OMI}(i, yr, m)$, $\Omega_{TROPOMI}(i, yr, m)$is adjusted OMI, original OMI and original TROPOMI products for grid i at year yr season m, respectively. $\Delta\Omega_{weights}(i, m)$ represents the difference between OMI and TROPOMI at target resolution. This correction strategy preserves the spatial patterns and seasonal variability of the original satellite products while ensuring temporal continuity and consistency of satellite-derived chemical variables across the entire study period.

Aerosol Optical Depth (AOD) data, an important proxy for particulate matter, were sourced from MODIS product (MCD19A2CMG) at a resolution of 0.05° × 0.05° for 2005-2023. The frequent occurrence of clouds in optical remote sensing images hampers the detection of trace gases beneath the cloud layer, leading to gaps in satellite data. To address this challenge, we implemented the eXtreme Gradient Boosting (XGBoost) machine learning algorithm, known for its efficiency, to fill these gaps and obtain spatially comprehensive retrieval data. This gap-filling procedure improves the representativeness of aerosol-related information and reduces potential biases associated with uneven data availability.

Additionally, we also included NDVI (2005-2023, MCD19A3CMG) to account for vegetation cover, population density data (2005-2020, WorldPop, https://www.worldpop.org/) to capture human activity, land use data (2005-2022, MCD12C1, providing sub-pixel proportions of nine class in forests, shrublands, savannas, wetlands, croplands, urban, snow and ice, barren, water) to understand land cover changes, and road network density and Digital Elevation Model (DEM) to incorporate infrastructural and topographical influences.

To ensure consistency across all input variables, the higher spatial resolution variables were aggregated to a homogeneous 0.1° × 0.1° grid using averaging, while the lower spatial resolution variables were resampled to the same grid using bilinear interpolation. Bilinear interpolation estimates values at target grid cells by linearly weighting the four nearest neighboring grid points in both latitude and longitude directions, thereby providing a smooth spatial transition while preserving large-scale gradients and avoiding abrupt discontinuities. This approach is widely adopted in atmospheric and remote sensing applications for spatial resampling, as it balances computational efficiency with the need to retain spatial coherence. This harmonization process enables the seamless integration of multi-source datasets within the machine learning framework. These processed variables were then used for subsequent air pollution modeling. This diverse set of features enabled a comprehensive machine learning approach to modeling NO_2 concentrations, providing robust predictions across various spatial and temporal scales.

2.2 Air Transformer

This study applied an innovative deep learning model, the Air Transformer (AiT), to improve the accuracy of atmospheric pollutant concentration prediction. The AiT model is based on the Transformer architecture and is specifically designed to capture the spatiotemporal dependencies of atmospheric pollutants. The AiT model structure builds on the successful application of the Transformer in natural language processing, incorporating cross-channel self-attention alongside pixel self-attention and utilizing a decoder for enhanced prediction capabilities. The multi-dimensional attention mechanism enables the model to capture dependencies not only across temporal and spatial dimensions but also among data channels,

https://doi.org/10.5194/essd-2025-821
Preprint. Discussion started: 14 January 2026

such as different pollutant concentrations and meteorological parameters. Transformers have the advantage of having no recurrent units, and therefore require less training time than earlier recurrent neural architectures (RNNs) such as long short-term memory (LSTM) (Zhao et al., 2019; Liu et al., 2024).

The self-attention mechanism is the core component of the AiT model. For each input sequence, attention weights are generated by computing the dot product between the query, key, and value vectors. These weights are used to perform a weighted sum of the input sequence values, producing new feature representations. The self-attention mechanism further enhances the model's representational power by allowing it to simultaneously focus on different parts of the input data, capturing richer spatiotemporal dependencies. In this study, the AiT model establishes a robust global surface–column relationship by integrating variables related to pollutant transport, chemical transformation, and column density within approximately 20 km of each target grid, enabling the reconstruction of gapless daily surface NO_2 concentrations at a spatial resolution of 10 km.

Multi-source data were input into AiT as model features and labels. These data were pre-processed through feature extraction layers and then fed into the Transformer's encoder. The encoder comprises multiple self-attention layers and feedforward neural network layers. Utilizing the multi-head attention mechanism, it processes input data in parallel, capturing features at various temporal and spatial scales. The AiT model is trained using supervised learning, leveraging a large amount of historical data. The model's loss function comprises prediction errors (such as mean squared error (MSE), Root Mean Square Error (RMSE)) and regularization terms to ensure prediction accuracy and stability. To improve the model's generalization ability, we introduced a multi-task learning strategy which was detailed discussed in our previous work (Tao et al., 2024). Specifically, the model not only predicts pollutant concentrations but also simultaneously predicts related meteorological parameters and remote sensing observations. This multi-task learning strategy helps the model better understand the interrelationships between different variables, thereby enhancing prediction performance.

Model training was conducted for 300 epochs using the LAMB optimizer, which supports large batch sizes without sacrificing convergence performance, thereby accelerating training on large-scale datasets. A warmup learning rate schedule was applied, with the learning rate peaking at 0.001, and a batch size of 6,144 was used. An early stopping strategy was implemented and triggered after 30 consecutive epochs without improvement. To mitigate overfitting, dropout was applied within linear layers and self-attention modules, and a Gaussian Error Linear Unit (GeLU) activation function was employed throughout the network.

The AiT model was implemented and trained using the PyTorch framework. Prior to training, all input features were normalized across the entire dataset. Model performance was evaluated using both sample-based and site-based cross-validation approaches. In these evaluations, all samples and monitoring sites were randomly divided into five folds, with four folds used for training and one fold reserved for independent validation, allowing for a rigorous assessment of the model's spatiotemporal generalization capability.

https://doi.org/10.5194/essd-2025-821
Preprint. Discussion started: 14 January 2026

Open Access Earth System Science Data Discussions

2.3 Random- and Spatial-based cross-validation

The performance of our models was evaluated using two five-fold cross-validation approaches: random-based and spatial-based. The random-based approach involved 16,841,418 samples, with 3,368,283 samples used for validation in each fold. This approach ensures a comprehensive assessment of the model's predictive performance across diverse temporal and spatial conditions represented in the full dataset, effectively testing the model's ability to reproduce observed NO_2 variability under a wide range of atmospheric and environmental settings. By randomly partitioning samples, this strategy primarily evaluates the overall fitting accuracy and stability of the model when predicting NO_2 concentrations at locations and times similar to those seen during training.

In contrast, the spatial-based approach was designed to explicitly assess the model's spatial transferability. This evaluation included data from 7,021 monitoring sites, of which 1,404 sites were held out for validation in each fold. By withholding entire monitoring locations from the training process, this approach tests the model's ability to generalize to previously unseen locations, which is critical for producing reliable spatially continuous NO_2 fields, particularly in regions with sparse or no ground observations. This site-based validation provides a more stringent and realistic assessment of model performance for global-scale mapping applications.

In both cross-validation approaches, validation data were strictly excluded from model training, ensuring an unbiased evaluation of predictive performance. Together, the random-based and spatial-based cross-validation strategies provide complementary perspectives on model accuracy and generalization capability, with the former primarily reflecting interpolation performance within the sampled space–time domain and the latter evaluating extrapolation ability to unmonitored locations. This combined evaluation framework is particularly well suited for global NO_2 mapping applications, where reliable prediction in regions with limited observational constraints is essential.

2.4 Regional weighted averages

To accurately assess regional pollution levels and the potential health impacts, we employ two complementary weighted averaging methods: geographically area-weighted averaging (Eq. (3)) and population-weighted averaging (Eq. (4)). These equations incorporate spatial area and population data to produce weighted averages that more accurately reflect both geographical and demographic factors in regional NO_2 concentration assessments.

$$C_{area-weighted} = \frac{\sum_{i=1}^{n} C_i \times A_i}{\sum_{i=1}^{n} A_i}, \quad (3)$$

where C_i is the NO_2 concentration in the ith region, A_i is the area of the ith region, and n is the total number of regions.

$$C_{population-weighted} = \frac{\sum_{i=1}^{n} C_i \times P_i}{\sum_{i=1}^{n} P_i}, \quad (4)$$

where C_i is the NO_2 concentration in the ith region, P_i is the population of the ith region, and n is the total number of regions. We used WorldPOP population datasets for this study. Population-weighted NO_2 concentration is a crucial indicator for

https://doi.org/10.5194/essd-2025-821
Preprint. Discussion started: 14 January 2026

assessing the public health impact of air pollution, as it integrates both pollutant concentration levels and the distribution of human populations across different regions. This metric is particularly useful for capturing the actual exposure of populations to NO_2 pollution, which is not adequately represented by area-weighted concentrations alone. By incorporating population density, the population-weighted NO_2 concentration metric provides a more accurate reflection of the exposure risk faced by people living and working in polluted areas.

3 Results

3.1 AiT-NO_2 performance

The detailed discussion about the Transformer can be seen in the Methods. Here we mainly focus on the performance evaluation from the AiT-NO_2 products. We first evaluate the model using Random cross-validation and Spatial cross-validation. In the Random cross-validation, the NO_2 model exhibited outstanding predictive accuracy, with an R^2 of 0.91, an RMSE of 2.32 ppbv, and an MAE of 1.56 ppbv for daily predictions (Fig. 1a). The performance further improved for monthly and annual predictions, achieving R^2 values of 0.98 and 0.99, RMSE values of 0.97 ppbv and 0.59 ppbv, and MAE values of 0.64 ppbv and 0.33 ppbv, respectively (Fig. 1c, e). This improvement reflects the reduction of short-term noise and random variability through temporal aggregation, indicating that the model effectively captures both high-frequency variability and long-term NO_2 signals.

Similarly, the Spatial cross-validation results were also impressive. For daily predictions, the NO_2 model achieved an R^2 of 0.62, an RMSE of 4.77 ppbv, and an MAE of 3.31 ppbv (Fig. 1b). For monthly and annual predictions, the model showed R^2 values of 0.65 and 0.63, RMSE values of 3.92 ppbv and 3.64 ppbv, and MAE values of 2.71 ppbv and 2.51 ppbv, respectively (Fig. 1d, f). As expected, predictive performance under Spatial cross-validation is lower than that under Random cross-validation, reflecting the greater difficulty of extrapolating to previously unseen locations. Nevertheless, the relatively stable performance across temporal scales indicates that the model maintains robust spatial transferability and is capable of reproducing NO_2 variability in regions with limited or no monitoring coverage.

Overall, the performance metrics obtained from both validation strategies demonstrate that the AiT-NO_2 model performs consistently well across multiple temporal scales and validation settings. The Spatial cross-validation results are generally comparable to, or exceed, those reported in previous global and regional NO_2 modeling studies (Wei et al., 2019; Wei et al., 2023), underscoring the robustness and reliability of the AiT-based framework for constructing spatially continuous, long-term NO_2 datasets.

https://doi.org/10.5194/essd-2025-821
Preprint. Discussion started: 14 January 2026

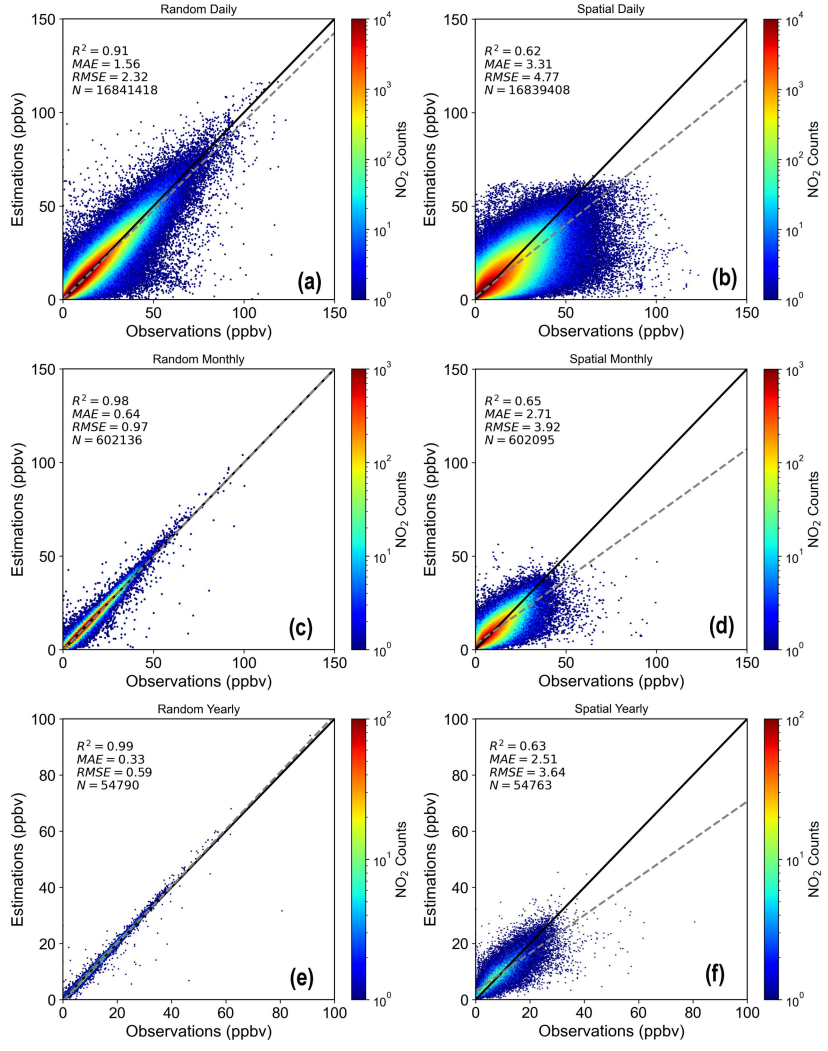

Figure 1: Model validation and uncertainties from the Random-based (left) and Spatial-based (right) cross-validation. Black lines are 1:1 lines, and grey dashed lines are best-fit lines from linear regression. Additional statistical metrics given are the correlation coefficient (R^2), mean absolute error (MAE), root-mean-square error (RMSE) and sample number.

As we mentioned earlier, the SoGA2024 for the first time included NO_2 in its report, as well as the annual NO_2 concentration datasets they generated using a global LUR model (Anenberg et al., 2022). The detailed methodology is available in Larkin et al. (Anenberg et al., 2022). Here, we mainly focus on the performance of the two datasets in simulating NO_2 concentration in major urban observation sites in several observation-dense countries, such as Austria, Belgium, China, France, Germany, India, Poland, Spain, and US. Overall, the AiTNO$_2$ model shows much better alignment with observational values, outperforming the LUR model. In most countries, except the US, predictions from the AiTNO$_2$ model tend to be slightly higher or almost comparable to the observational data, whereas the LUR model consistently underestimates NO_2 concentrations. For countries like China and India, where pollution levels are particularly high, the AiTNO$_2$ model provides

https://doi.org/10.5194/essd-2025-821
Preprint. Discussion started: 14 January 2026

significantly more accurate predictions, closely reflecting the actual pollution patterns observed in these regions. This highlights the efficacy of the AiTNO$_2$ model. We estimated that the LUR method could significantly underestimate the regional NO$_2$ concentration by at least 50% for most of the regions, except for HI (Supplement Fig. S3; Table S2). When examining different regions, our results has much higher NO$_2$ estimation compared to LUR NO$_2$, particularly in the Northern Hemisphere (1.6 to 2.1 times) and tropical regions (2.5 to 3.0 times), where there are more monitoring stations and higher pollution levels (Supplementary Fig. S4). The primary reason for this discrepancy is that the AiTNO$_2$ model relies on urban stations data for training, which are typically located in city centres with high pollution levels, enabling it to more effectively capture elevated NO$_2$ concentrations in these localized urban areas. In contrast, the LUR model, which utilizes lower-resolution land use variables and satellite data, is less capable of fully reflecting high NO$_2$ concentration areas, especially in urban settings. Furthermore, the AiTNO$_2$ model was featured in higher sensitivity in capturing the temporal and spatial variations of atmospheric pollutants, accurately predicting these changes by learning from time series data (Tao et al., 2024). In conclusion, both cross-validation approaches confirm the strong predictive capabilities of our model. The Random validation highlights the model's accuracy across diverse data points, while the Spatial validation underscores its effectiveness in generalizing to new locations. These comprehensive evaluations attest to the high quality and reliability of our predictive models, making them valuable tools for accurate NO$_2$ concentration predictions. The AiTNO$_2$ model shows higher accuracy in predicting NO$_2$ concentrations across the selected countries, especially in regions with severe pollution and dense monitoring networks. While the LUR model captures the general trends in NO$_2$ variation, its predictions are often conservative and fail to adequately represent pollution levels in some countries, particularly in high-pollution areas. The AiTNO$_2$ model, by leveraging deep learning and observational data, compensates for these limitations and demonstrates its potential as a valuable tool for air pollution monitoring and forecasting. These advantages highlight the value of the AiT-based approach for constructing high-resolution global NO$_2$ datasets and for improving the representation of surface NO$_2$ concentrations in data-driven air quality analyses.

3.2 Global Trend of NO$_2$

Based on the geographically area-weighted average AiTNO$_2$, we have a systematic understanding of the global spatial and temporal trends in NO$_2$. The global annual average concentration of NO$_2$ exhibited distinct trends among regions from 2005 to 2023 (Supplementary Fig. S5a). Specifically, from 2005 to 2010, NO$_2$ concentrations remained relatively stable, increasing slightly from 3.32 ppbv to 3.44 ppbv. From 2010 to 2015, concentrations continued to rise, peaking at 4.05 ppbv in 2015. Subsequently, despite a decrease to 3.73 ppbv by 2019, concentrations remained relatively high. In 2020, due to the significant reduction in global economic activities and transportation caused by the COVID-19 pandemic, NO$_2$ concentrations notably dropped to 3.42 ppbv. From 2021 to 2023, with the gradual recovery of economic activities, NO$_2$ concentrations rebounded slightly in 2021 but then declined again in 2022 and 2023, reaching 3.38 ppbv in 2023. Figures S5b and S5c show that the NO$_2$ concentrations in the Northern Hemisphere and tropical regions exhibited similar trends. In contrast to global trends, the Southern Hemisphere exhibited unique characteristics in the annual average NO$_2$ concentrations

https://doi.org/10.5194/essd-2025-821
Preprint. Discussion started: 14 January 2026

from 2005 to 2023 (Supplementary Fig. S5d). Between 2005 and 2009, NO_2 levels decreased from 2.83 ppbv to 2.66 ppbv, likely due to the initial implementation of air pollution control measures in certain regions. From 2010 to 2015, NO_2 concentrations fluctuated, overall declining from 2.68 ppbv to 2.65 ppbv. This period's fluctuations may reflect the dynamic balance between economic activities and air quality management policies. Between 2016 and 2019, NO_2 levels remained relatively stable, ranging from 2.63 ppbv to 2.69 ppbv, indicating a balance between ongoing mitigation efforts and economic growth. In 2020, the COVID-19 pandemic led to a significant reduction in economic activities and transportation, causing NO_2 concentrations to drop sharply to 2.45 ppbv, highlighting the substantial impact of anthropogenic activities on NO_2 emissions. From 2021 to 2023, as economic activities gradually resumed, NO_2 levels increased markedly, reaching 3.15 ppbv in 2022 before slightly declining to 3.11 ppbv in 2023. This upward trend is likely associated with economic recovery, increased traffic, and the relaxation of emission control measures in some areas. Overall, these results highlight pronounced regional differences in long-term NO_2 evolution and underscore the combined influence of anthropogenic activity, emission control measures, and large-scale external perturbations on global and hemispheric NO_2 concentrations.

3.3 Spatial and Temporal Trends based on AiTNO$_2$

We examine the spatial distribution and regional evolution of NO_2 concentrations from 2005 to 2023 to characterize geographic heterogeneity and regional hotspots. Significant spatial heterogeneous in NO_2 concentration across regions have been identified from 2005 to 2023 (Fig. S7), with hotspots in eastern China and northern India. In 2005, regions including the Beijing-Tianjin-Hebei area and the Yangtze River Delta exhibited very high NO_2 concentrations due to their status as major industrial and economic centres. However, after 2013, these regions experienced significant reductions in NO_2 levels, largely attributed to the Chinese government's stringent air quality management policies, including the Air Pollution Prevention and Control Action Plan, which effectively reduced industrial emissions and vehicle exhaust (Feng et al., 2019; Liu et al., 2024; Gao et al., 2022; Geng et al., 2019). In India, NO_2 hotspots are concentrated in major cities located in the Indo-Gangetic Plain such as Delhi and Mumbai. Between 2005 and 2015, NO_2 concentrations in these cities gradually increased due to rapid urbanization and industrialization. However, recent years have seen a decrease in NO_2 levels as the Indian government has intensified efforts to control air pollution (Xie et al., 2024). Conversely, Western European countries like Germany, France, and the United Kingdom had high NO_2 concentrations in 2005, reflecting their industrialized cities and busy transportation networks, and then significantly decreased due to the European Union's strict emission standards and air quality regulations (Guerreiro et al., 2014; Sicard et al., 2021; Georgoulias et al., 2019; Crippa et al., 2016). In North America, the northeastern industrial corridor of the US and Canada, along with major cities like Los Angeles and New York, shared a similar pattern as Western European countries. While overall NO_2 concentrations are lower in Africa and South America, industrial centres and major cities like Johannesburg in South Africa and Sao Paulo in Brazil have shown increased NO_2 levels in certain years. These areas require further pollution control measures to improve air quality.

https://doi.org/10.5194/essd-2025-821
Preprint. Discussion started: 14 January 2026

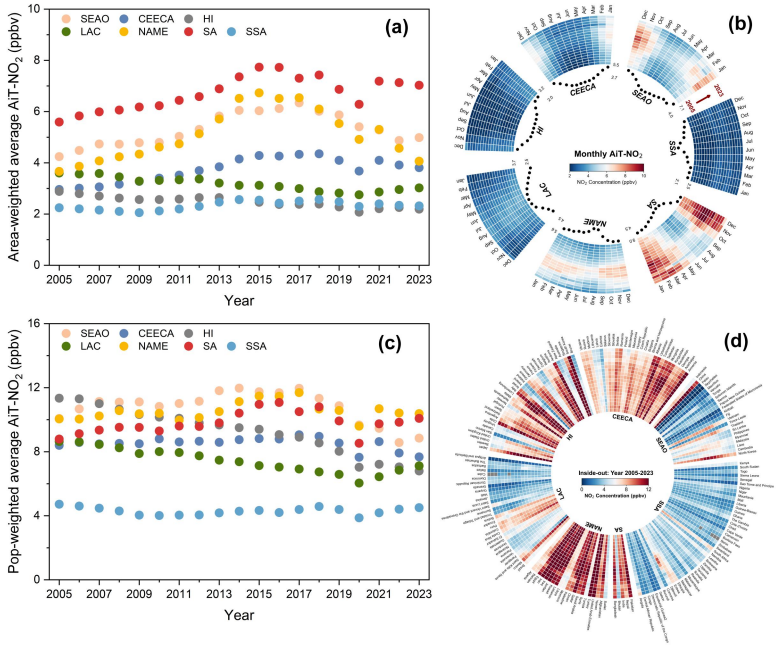

Figure 2: Temporal trends of annual NO_2 concentration from 2005 to 2023 in seven GBD super-regions for a) area-weighted average; c) population-weighted average. b) Heatmap of monthly area-weighted average, with scatter plots indicating monthly averages over the 19-year period. d) Heatmap of annual population-weighted average NO_2 concentrations for each country within the super-regions from 2005 to 2023. The seven super-regions defined in GBD are South-East Asia, East Asia & Oceania (SEAO), Central Europe, Eastern Europe & Central Asia (CEECA), High-income (HI), Latin America & Caribbean (LAC), North Africa & Middle East (NAME), South Asia (SA), and Sub-Saharan Africa (SSA).

We further discussed the annual NO_2 changes in seven super-regions (Fig. 2a, b) following the definitions by Global Burden of Disease (GBD) (Fig. S2): South-East Asia, East Asia & Oceania (SEAO), Central Europe, Eastern Europe & Central Asia (CEECA), High-income (HI), Latin America & Caribbean (LAC), North Africa & Middle East (NAME), South Asia (SA), and Sub-Saharan Africa (SSA). SA region has consistently the highest area-weighted NO_2 levels among all regions, followed by SEAO and NAME. NO_2 concentrations in these regions, as well as in CEECA, showed an increasing trend until 2015. In SA, SEAO, and NAME, the rise was primarily driven by rapid industrialization, urbanization, and increased transportation demand, while in CEECA, the increase was also linked to a reliance on fossil fuels and slower implementation of emission control measures. After 2015, NO_2 levels began to stabilize or decline due to local emission reduction efforts and global events like the COVID-19 pandemic.

In contrast, $AiTNO_2$ concentrations in other super-regions (LAC, HI, and SSA) are relatively low, with annual averages of less than 4 ppbv for the past two decades (Fig. 2a). The LAC region benefits from a combination of lower vehicle density in rural areas and successful urban air quality initiatives in major cities (Riojas-Rodríguez et al., 2016; Huneeus et al., 2020). The lower NO_2 levels in the HI region are largely due to stringent environmental regulations, advanced pollution control technologies, and a significant shift towards cleaner energy sources. SSA presents a unique case where low industrialization

https://doi.org/10.5194/essd-2025-821
Preprint. Discussion started: 14 January 2026

Open Access Earth System Science Data Discussions

and vehicle ownership contribute to lower NO_2 levels. However, the region is still impacted by biomass burning for cooking and heating, which can lead to localized spikes in NO_2 (Fig. S7).

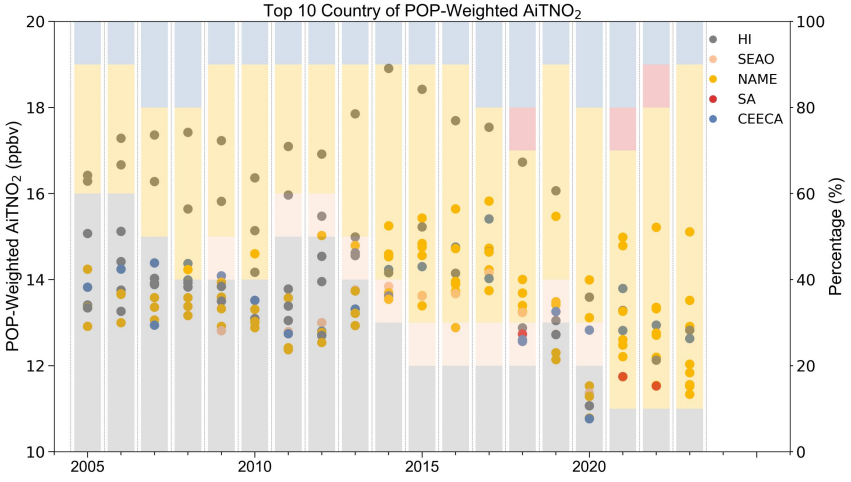

Figure 3: Top 10 countries ranked by population-weighted NO_2 concentration (2005-2023) and their regional distribution. The left y-axis corresponds to the scatter plot, representing population-weighted $AiTNO_2$ concentrations in parts per billion by volume (ppbv) for each country. The right y-axis corresponds to the background colors, which represent the proportion of countries from different super-regions (HI, SEAO, NAME, SA, and CEECA) that are ranked in the top 10 based on $AiTNO_2$ concentration. The background color segments show the percentage of top 10 countries that belong to each region, reflecting how the regional representation in the top 10 has evolved over time.

When considering the population exposure, we found that high levels of NO_2 were also observed in some developed regions, such as HI (including North America, Western Europe, Southern Latin America, Asia Pacific, and Australasia), which ranked first among the seven super-regions from 2005 to 2007 (Fig. 2c; Fig. S9). The higher population-weighted average of NO_2 in HI was mainly attributed to several population dense countries, including South Korea, Japan, Singapore, Andorra, Germany and Italy (Fig. 2d; Fig. S9). Figure 3 illustrates the proportion of super regions that include the top ten countries with the highest population-weighted NO_2 exposure over the past two decades. During the early years of the study period, the HI region accounted for 60% of the top ten countries in terms of NO_2 exposure. However, this proportion gradually decreased, leaving only one country from the HI region among the top ten in recent years. In contrast, the NAME region experienced a sharp increase in its share of countries with high NO_2 exposure, eventually becoming the predominant area for such countries. This shift underscores the dynamic nature of NO_2 exposure distribution, influenced by both changes in NO_2 emissions and population dynamics.

We estimated that in recent years, SEAO, NAME, and SA are among the top regions with the highest population-weighted NO_2 concentration, with multiple year average of 10.78 ± 1.02 ppbv, 10.54 ± 0.55 ppbv, 9.81 ± 0.70 ppbv from 2005 to 2023, respectively. NO_2 exposure was increasing by 0.19 and 0.72 ppbv/decade in NAME and SA, while decreasing by 0.68, 0.40, 2.53, 0.85, 0.12 ppbv/decade in SEAO, CEECA, HI, LAC, and SSA, respectively (Fig. 2c). These contrasting trends highlight substantial temporal changes in population-weighted NO_2 distributions across super-regions, reflecting the combined influence of evolving emission patterns and regional population dynamics.

https://doi.org/10.5194/essd-2025-821
Preprint. Discussion started: 14 January 2026

4 Data availability

The global NO_2 dataset developed using the Air Transformer (AiT) framework is available at: https://doi.org/10.5281/zenodo.13842191 (Mu and Tao, 2025).

5 Discussion and conclusion

This study delivers a long-term, spatially consistent global nitrogen dioxide (NO_2) data resource that supports systematic analyses of NO_2 variability and evolution across regions with contrasting emission characteristics. By providing a unified representation of surface NO_2 concentrations over nearly two decades, the dataset enables comparative investigations of regional patterns and temporal changes and facilitates intercomparison with existing observation- and model-based products. As a globally consistent data foundation, it helps improve the coherence of long-term NO_2 analyses across different geographic and climatic regimes and provides valuable insights for future epidemiological research. In addition, the dataset may facilitate downstream assessments that relate NO_2 distributions to commonly used guideline values.

This dataset consists of high-resolution global daily surface NO_2 concentrations for the period 2005–2023, generated using the Air Transformer (AiT) deep learning model. The dataset represents a major advancement in air quality research by overcoming the limitations of traditional ground-based monitoring networks and providing a fine-scale temporal resolution capable of capturing daily variations in NO_2 concentrations. Such high-frequency data is crucial for understanding the short-term dynamics of NO_2 pollution, which are often influenced by transient meteorological conditions, industrial emissions, and traffic patterns. The model's robust validation against independent datasets demonstrates its reliability and predictive performance, offering a more detailed depiction of NO_2 pollution trends across diverse geographical regions, including both densely populated urban areas and remote locations with limited observational data.

The implications of this work extend far beyond conventional air quality monitoring. The dataset provides a valuable resource for assessing the localized impacts of anthropogenic activities, such as industrial production and urban development, as well as the effectiveness of pollution control measures. This fine-grained understanding of NO_2 distribution is particularly critical in densely populated areas, where exposure to elevated NO_2 levels poses significant public health risks, including respiratory and cardiovascular diseases. The dataset's high spatial and temporal resolution enhances the precision of exposure assessments, supporting epidemiological studies and the formulation of targeted public health interventions.

Furthermore, the framework established in this study has the potential to be adapted and extended for the monitoring of other air pollutants, such as ozone (O_3) and fine particulate matter ($PM_{2.5}$), which also exhibit significant spatial and temporal variability. This versatility underscores the broader applications of the AiT model in environmental policy and public health management. By enabling more accurate and granular assessments of air quality, this dataset can inform regulatory actions and contribute to the development of more effective strategies for mitigating air pollution and protecting human health.

https://doi.org/10.5194/essd-2025-821
Preprint. Discussion started: 14 January 2026

Future work should focus on expanding data sources, such as emissions inventories and traffic data, to further improve the model's accuracy, especially in less urbanized regions, enabling more comprehensive global assessments of NO_2 pollution and contributing to the development of more targeted and effective air quality management strategies.

Author contributions

YQZ conceived the study, and reviewed and edited the manuscript. LX secured project funding and reviewed the manuscript. JM drafted the original manuscript, contributed to methodology development and visualization, refined the methods, and edited the manuscript. CT contributed to methodology development and visualization and refined the methods. ZL, YNZ, NZ, BL, and QHZ contributed to methodology development. QZZ and HZ reviewed the manuscript. JM and CT contributed equally to this work.

Competing interests

At least one of the (co-)authors is a member of the editorial board of Earth System Science Data.

Financial support

This work was funded by Development Program of the Ministry of Science and Technology of China (grant no. 2022YFC3701101).

References

Anenberg, S. C., Mohegh, A., Goldberg, D. L., Kerr, G. H., Brauer, M., Burkart, K., Hystad, P., Larkin, A., Wozniak, S., and Lamsal, L.: Long-term trends in urban NO_2 concentrations and associated paediatric asthma incidence: estimates from global datasets, Lancet Planet. Health, 6, e49–e58, https://doi.org/10.1016/S2542-5196(21)00255-2, 2022.

Chan, K. L., Khorsandi, E., Liu, S., Baier, F., and Valks, P.: Estimation of surface NO_2 concentrations over Germany from TROPOMI satellite observations using a machine learning method, Remote Sens., 13, 969, https://doi.org/10.3390/rs13050969, 2021.

https://doi.org/10.5194/essd-2025-821
Preprint. Discussion started: 14 January 2026

Chi, Y., Fan, M., Zhao, C., Yang, Y., Fan, H., Yang, X., Yang, J., and Tao, J.: Machine learning-based estimation of ground-level NO_2 concentrations over China, Sci. Total Environ., 807, 150721, https://doi.org/10.1016/j.scitotenv.2021.150721, 2022.

Cooper, M. J., Martin, R. V., Hammer, M. S., Levelt, P. F., Veefkind, P., Lamsal, L. N., Krotkov, N. A., Brook, J. R., and McLinden, C. A.: Global fine-scale changes in ambient NO_2 during COVID-19 lockdowns, Nature, 601, 380–387, https://doi.org/10.1038/s41586-021-04229-0, 2022.

Crippa, M., Janssens-Maenhout, G., Dentener, F., Guizzardi, D., Sindelarova, K., Muntean, M., Van Dingenen, R., and Granier, C.: Forty years of improvements in European air quality: regional policy-industry interactions with global impacts, Atmos. Chem. Phys., 16, 3825–3841, https://doi.org/10.5194/acp-16-3825-2016, 2016.

Di, Q., Amini, H., Shi, L., Kloog, I., Silvern, R., Kelly, J., Sabath, M. B., Choirat, C., Koutrakis, P., and Lyapustin, A.: Assessing NO_2 concentration and model uncertainty with high spatiotemporal resolution across the contiguous United States using ensemble model averaging, Environ. Sci. Technol., 54, 1372–1384, https://doi.org/10.1021/acs.est.9b03358, 2019.

Feng, Y., Ning, M., Lei, Y., Sun, Y., Liu, W., and Wang, J.: Defending blue sky in China: effectiveness of the "Air Pollution Prevention and Control Action Plan" on air quality improvements from 2013 to 2017, J. Environ. Manage., 252, 109603, https://doi.org/10.1016/j.jenvman.2019.109603, 2019.

Gao, J., Yang, Y., Wang, H., Wang, P., Li, H., Li, M., Ren, L., Yue, X., and Liao, H.: Fast climate responses to emission reductions in aerosol and ozone precursors in China during 2013–2017, Atmos. Chem. Phys., 22, 7131–7142, https://doi.org/10.5194/acp-22-7131-2022, 2022.

Geng, G., Xiao, Q., Zheng, Y., Tong, D., Zhang, Y., Zhang, X., Zhang, Q., He, K., and Liu, Y.: Impact of China's air pollution prevention and control action plan on $PM_{2.5}$ chemical composition over eastern China, Sci. China Earth Sci., 62, 1872–1884, https://doi.org/10.1007/s11430-018-9353-x, 2019.

Georgoulias, A. K., van der A, R. J., Stammes, P., Boersma, K. F., and Eskes, H. J.: Trends and trend reversal detection in 2 decades of tropospheric NO_2 satellite observations, Atmos. Chem. Phys., 19, 6269–6294, https://doi.org/10.5194/acp-19-6269-2019, 2019.

Guerreiro, C. B., Foltescu, V., and De Leeuw, F.: Air quality status and trends in Europe, Atmos. Environ., 98, 376–384, https://doi.org/10.1016/j.atmosenv.2014.09.017, 2014.

Health Effects Institute: State of Global Air 2024; Special Report; Health Effects Institute, Boston, MA, https://www.stateofglobalair.org, 2024.

Huang, K., Xiao, Q., Meng, X., Geng, G., Wang, Y., Lyapustin, A., Gu, D., and Liu, Y.: Predicting monthly high-resolution $PM_{2.5}$ concentrations with random forest model in the North China Plain, Environ. Pollut., 242, 675–683, https://doi.org/10.1016/j.envpol.2018.07.016, 2018.

Huang, K., Zhu, Q., Lu, X., Gu, D., and Liu, Y.: Satellite-based long-term spatiotemporal trends in ambient NO_2 concentrations and attributable health burdens in China from 2005 to 2020, GeoHealth, 7, e2023GH000798, https://doi.org/10.1029/2023GH000798, 2023.

https://doi.org/10.5194/essd-2025-821
Preprint. Discussion started: 14 January 2026

Huneeus, N., van Der Gon, H. D., Castesana, P., Menares, C., Granier, C., Granier, L., Alonso, M., de Fatima Andrade, M., Dawidowski, L., and Gallardo, L.: Evaluation of anthropogenic air pollutant emission inventories for South America at national and city scale, Atmos. Environ., 235, 117606, https://doi.org/10.1016/j.atmosenv.2020.117606, 2020.

Levelt, P. F., Van Den Oord, G. H., Dobber, M. R., Malkki, A., Visser, H., De Vries, J., Stammes, P., Lundell, J. O., and Saari, H.: The ozone monitoring instrument, IEEE Trans. Geosci. Remote Sens., 44, 1093–1101, https://doi.org/10.1109/TGRS.2006.872333, 2006.

Li, K., Jacob, D. J., Liao, H., Shen, L., Zhang, Q., and Bates, K. H.: Anthropogenic drivers of 2013–2017 trends in summer surface ozone in China, Proc. Natl. Acad. Sci. U.S.A., 116, 422–427, https://doi.org/10.1073/pnas.1812168116, 2019.

Liu, R., Shao, M., and Wang, Q.: Multi-timescale variation characteristics of $PM_{2.5}$ in different regions of China during 2014–2022, Sci. Total Environ., 920, 171008, https://doi.org/10.1016/j.scitotenv.2024.171008, 2024.

Liu, X., Zhang, X., Wang, R., Liu, Y., Hadiatullah, H., Xu, Y., Wang, T., Bendl, J., Adam, T., and Schnelle-Kreis, J.: High-precision microscale particulate matter prediction in diverse environments using a Long Short-Term Memory neural network and street view imagery, Environ. Sci. Technol., 58, 3869–3882, https://doi.org/10.1021/acs.est.3c06511, 2024.

Long, S., Wei, X., Zhang, F., Zhang, R., Xu, J., Wu, K., Li, Q., and Li, W.: Estimating daily ground-level NO_2 concentrations over China based on TROPOMI observations and machine learning approach, Atmos. Environ., 289, 119310, https://doi.org/10.1016/j.atmosenv.2022.119310, 2022.

Mu, J. and Tao, C.: GlobalNO2_AIT: 0.1° annual resolution global ground-level NO_2 dataset, Zenodo, https://doi.org/10.5281/zenodo.13842191, 2025.

Riojas-Rodríguez, H., da Silva, A. S., Texcalac-Sangrador, J. L., and Moreno-Banda, G. L.: Air pollution management and control in Latin America and the Caribbean: implications for climate change, Rev. Panam. Salud Pública, 40, 150–159, 2016.

Sekiya, T., Miyazaki, K., Eskes, H., Sudo, K., Takigawa, M., and Kanaya, Y.: A comparison of the impact of TROPOMI and OMI tropospheric NO_2 on global chemical data assimilation, Atmos. Meas. Tech., 15, 1703–1728, https://doi.org/10.5194/amt-15-1703-2022, 2022.

Sicard, P., Agathokleous, E., De Marco, A., Paoletti, E., and Calatayud, V.: Urban population exposure to air pollution in Europe over the last decades, Environ. Sci. Eur., 33, 1–12, https://doi.org/10.1186/s12302-020-00450-2, 2021.

Tao, C., Peng, Y., Zhang, Q., Zhang, Y., Gong, B., Wang, Q., and Wang, W.: Diagnosing ozone–NO_x–VOC–aerosol sensitivity and uncovering causes of urban–nonurban discrepancies in Shandong, China, using transformer-based estimations, Atmos. Chem. Phys., 24, 4177–4192, https://doi.org/10.5194/acp-24-4177-2024, 2024.

Veefkind, J. P., Aben, I., McMullan, K., Förster, H., De Vries, J., Otter, G., Claas, J., Eskes, H., De Haan, J., and Kleipool, Q.: TROPOMI on the ESA Sentinel-5 Precursor: A GMES mission for global observations of the atmospheric composition for climate, air quality and ozone layer applications, Remote Sens. Environ., 120, 70–78, https://doi.org/10.1016/j.rse.2011.09.027, 2012.

https://doi.org/10.5194/essd-2025-821
Preprint. Discussion started: 14 January 2026

Wei, J., Huang, W., Li, Z., Xue, W., Peng, Y., Sun, L., and Cribb, M.: Estimating 1-km-resolution $PM_{2.5}$ concentrations across China using the space-time random forest approach, Remote Sens. Environ., 231, 111221, https://doi.org/10.1016/j.rse.2019.111221, 2019.

Wei, J., Li, Z., Chen, X., Li, C., Sun, Y., Wang, J., Lyapustin, A., Brasseur, G. P., Jiang, M., and Sun, L.: Separating daily 1 km $PM_{2.5}$ inorganic chemical composition in China since 2000 via deep learning integrating ground, satellite, and model data, Environ. Sci. Technol., 57, 18282–18295, https://doi.org/10.1021/acs.est.3c00272, 2023.

Wong, P.-Y., Su, H.-J., Lee, H.-Y., Chen, Y.-C., Hsiao, Y.-P., Huang, J.-W., Teo, T.-A., Wu, C.-D., and Spengler, J. D.: Using land-use machine learning models to estimate daily NO_2 concentration variations in Taiwan, J. Clean. Prod., 317, 128411, https://doi.org/10.1016/j.jclepro.2021.128411, 2021.

Xie, Y., Zhou, M., Hunt, K. M., and Mauzerall, D. L.: Recent $PM_{2.5}$ air quality improvements in India benefited from meteorological variation, Nat. Sustain., 1–11, https://doi.org/10.1038/s41893-024-01366-y, 2024.

Xue, L., Wang, T., Gao, J., Ding, A., Zhou, X., Blake, D., Wang, X., Saunders, S., Fan, S., and Zuo, H.: Ground-level ozone in four Chinese cities: precursors, regional transport and heterogeneous processes, Atmos. Chem. Phys., 14, 13175–13188, https://doi.org/10.5194/acp-14-13175-2014, 2014.

Zhao, Y., Wang, L., Luo, J., Huang, T., Tao, S., Liu, J., Yu, Y., Huang, Y., Liu, X., and Ma, J.: Deep learning prediction of polycyclic aromatic hydrocarbons in the high arctic, Environ. Sci. Technol., 53, 13238–13245, https://doi.org/10.1021/acs.est.9b05000, 2019.